CrossMark

On the Statistics of Elsasser Increments in Solar Wind and Magnetohydrodynamic Turbulence

Juan C. Palacios[1] ⬤, Sofiane Bourouaine[2] ⬤, and Jean C. Perez[1] ⬤

[1] Department of Aerospace, Physics and Space Sciences, Florida Institute of Technology, 150 University Boulevard, Melbourne, FL 32901, USA
jpalacioscai2014@my.fit.edu

[2] Johns Hopkins University Applied Physics Laboratory, Laurel, MD, USA

Abstract

In this Letter we investigate the dependency with scale of the empirical probability distribution functions (PDF) of Elsasser increments using large sets of *WIND* data (collected between 1995 and 2017) near 1 au. The empirical PDF are compared to the ones obtained from high-resolution numerical simulations of steadily driven, homogeneous reduced MHD turbulence on a 2048^3 rectangular mesh. A large statistical sample of Alfvénic increments is obtained by using conditional analysis based on the solar wind average properties. The PDF tails obtained from observations and numerical simulations are found to have exponential behavior in the inertial range, with an exponential decrement that satisfies power laws of the form $\alpha_l \propto l^{-\mu}$, where l is the scale size, with μ between 0.17 and 0.25 for observations and 0.43 for simulations. PDF tails were extrapolated assuming their exponential behavior extends to arbitrarily large increments in order to determine structure function scaling laws at very high orders. Our results point to potentially universal scaling laws governing the PDF of Elsasser increments and to an alternative approach to investigate high-order statistics in solar wind observations.

Unified Astronomy Thesaurus concepts: Magnetohydrodynamics (1964); Interplanetary turbulence (830); Solar wind (1534)

1. Introduction

Decades of spacecraft observations have shown that the solar wind properties exhibit random fluctuations over a wide range of lengthscales consistent with a turbulent state (Bruno & Carbone 2013). For scales larger than any plasma microscale, such as the ion and electron gyroradius, the power spectra of velocity and magnetic fluctuations obeys a power law similar to the Kolmogorov $k^{-5/3}$ law for fluid turbulence (Kolmogorov 1941a, 1941b; K41 hereafter), which has long been thought to arise from an incompressible Magnetohydrodynamics (MHD) turbulent cascade mediated by Alfvénic fluctuations (Coleman 1968; Belcher et al. 1969).

Since the pioneering work of Iroshnikov (1963, 1964) and Kraichnan (1965; IK hereafter), predicting a power spectrum scaling $\propto k^{-3/2}$, most MHD turbulence models (Goldreich & Sridhar 1995; Lithwick et al. 2007; Chandran 2008; Beresnyak & Lazarian 2008; Boldyrev 2005; Perez & Boldyrev 2009) are based on Kolmogorov's assumption that the spatial distribution of fluctuations is self-similar in the inertial range. Self-similarity is intuitively associated with the fact that fluctuations at each scale $l \sim 1/k$ are space filling. However, fluid turbulence experiments and simulations (Anselmet et al. 1984; Gotoh et al. 2002), and solar wind observations (Burlaga 1991) show that at smaller scales the distribution of turbulent fluctuations becomes increasingly sparse. This departure from self-similarity, which is called intermittency, plays an important role in plasma heating processes (Sundkvist et al. 2007; Zhdankin et al. 2016).

The first observations of intermittency in the solar wind by Burlaga (1991) were followed by numerous works on the subject using nearly every spacecraft to date, for a recent review see Bruno (2019). The large majority of these works have focused on the intermittency of velocity v and magnetic field B. However, the so-called Elsasser fields $z^{\pm} = v \pm B / \sqrt{4\pi\rho}$ (Elsasser 1950) are more fundamental variables in MHD turbulence given that, contrary to kinetic and magnetic energy, their energies are subject to a conservative cascade. In this work we use the largest statistical sample to date of turbulent increments in the solar wind from the *WIND* spacecraft, spanning 23 yr from 1995 to 2017, and from high-resolution numerical simulations of steadily driven MHD turbulence to investigate the scale-dependent probability distribution functions (PDF) of Elsasser increments. Our analysis is based on conditional statistics to ensure Elsasser increments belong to Alfvénic fluctuations. The large statistical sample allows us to empirically estimate the PDF of the turbulence increments over many standard deviations, capturing a significant portion of those heavy tails that are signature of intermittency. Exponential least square fits of these tails are obtained to investigate their dependency on the scale, which in turn we use to extrapolate empirical PDF to obtain estimates of structure functions to higher orders than those allowed by the finite data sample. These results show the first empirical evidence of potentially universal scaling laws governing the PDF tails of Elsasser increments in the solar wind, and enable a new venue to investigate intermittency that allows for direct comparisons with new and existing theoretical models.

This paper is organized as follows. In Section 2 we provide a brief theoretical background of intermittency in MHD and solar wind turbulence in order to provide minimal context and notation that will be used in the rest of this paper. In Section 3 we describe the solar wind observations from the *WIND* spacecraft and numerical simulations, as well as the methodology used in this work to obtain Elsasser increments and their corresponding PDF. In Section 4 we show and discuss our results and in Section 5 we present our conclusions.

2. Theoretical Framework

The statistical properties of MHD turbulence are often described in terms of the statistical moments of longitudinal increments (Biskamp & Müller 2000)

$$\delta z_L^\pm(\boldsymbol{l}, \boldsymbol{x}, t) = \hat{\boldsymbol{l}} \cdot \delta z^\pm(\boldsymbol{l}, \boldsymbol{x}, t), \qquad (1)$$

where $\delta z^\pm(\boldsymbol{l}, \boldsymbol{x}, t) \equiv z^\pm(\boldsymbol{x} + \boldsymbol{l}/2, t) - z^\pm(\boldsymbol{x} - \boldsymbol{l}/2, t)$ represent a typical turbulent fluctuation at scale $l = |\boldsymbol{l}|$, $\boldsymbol{l}$ represents a scale vector in the plane perpendicular to the mean background magnetic field, and $\hat{\boldsymbol{l}}$ is the unit vector in the direction of $\boldsymbol{l}$. In the homogeneous and stationary state, these moments, known as *structure functions*, are expected to satisfy universal power laws of the form

$$S_n^\pm(l) = \langle |\delta z_L^\pm(\boldsymbol{x}, \boldsymbol{l})|^n \rangle = a_n^\pm l^{\zeta_n^\pm}, \qquad (2)$$

for lengthscales l in the inertial range. In this expression, we use $\langle \cdots \rangle$ to denote a suitable ensemble average and $a_n^\pm$ are nonuniversal coefficients that solely depend on n.

Kolmogorov's self-similarity assumption implies that the scaling exponents $\zeta_n^\pm$ are linear in n

$$\zeta_n^\pm = h^\pm n, \qquad h > 0, \qquad (3)$$

where $h^\pm$ are constants. Although dimensional arguments can be used to uniquely determine $h = 1/3$ in fluids, they alone are not sufficient to determine $h^\pm$ in MHD. IK and K41 scaling correspond to $h^\pm = 1/4$ and $h^\pm = 1/3$, respectively.

Multifractality arises assuming that the turbulence cascade accumulates on multiple fractal sets with different fractal dimensions, resulting in a range of scaling exponents $h \in [h_{min}, h_{max}]$ in which fluctuations satisfy local scale invariance with the corresponding scaling index h. In this picture, the scaling of structure functions at each order n results from the fractal set with index h that has the most dominant contribution to the average of the nth order power of the corresponding increment. As a result, the dependency with n of the scaling exponents ζ_n becomes nonlinear, because at each n the largest contribution to the statistical average arises from a fractal set with a different h value.

Structure functions are defined in terms of hypothetical ensemble averages, which assume an arbitrarily large number of identical realizations of the system. In practice, an ergodicity assumption has to be invoked in the homogeneous and stationary state in order to empirically estimate these averages using a finite sample. In reality, an exact calculation of these structure functions is only possible if the PDF governing the increments were known, which provides the most comprehensive description of turbulence theory. The PDF $\mathscr{P}(u)$ of a random variable u is defined such that $\mathscr{P}(u)du$ is the probability of finding the random variable u between u and $u+du$. The structure functions can then be written in terms of the scale-dependent PDF $\mathscr{P}^\pm(u, l)$ associated with the corresponding Elsasser fields as

$$S_n^\pm(l) = \int_{-\infty}^{\infty} u^n \mathscr{P}^\pm(u, l) du, \qquad (4)$$

where u represents the increments of the fields. Note that in this work we define structure functions in terms of the increment magnitude $|u|$, which in general exhibit a more distinct scaling behavior and are expected to show the same exponents as the moments of u (Biskamp & Müller 2000). Performing a statistical study of increments using the PDF is an alternative venue to study intermittency in the inertial range (Sorriso-Valvo et al. 1999; Barndorff-Nielsen et al. 2004), which is one of the main objectives of this Letter.

3. Data and Methodology

We use data for density ρ, magnetic field $\boldsymbol{B}$, and velocity $\boldsymbol{v}$ from the *WIND* spacecraft. The 23 yr of data from the *WIND*/3DP instrument (3D plasma analyzer) with a resolution of $\sim$24 s were used. Velocity and magnetic field increments were carefully selected to ensure they belong to periods of homogeneous and incompressible turbulence in the slow and fast solar wind. For solar wind observations data were first resampled to a uniform grid of 24 s using linear interpolation and any gaps that the data may have were discarded. The local mean quantities $\rho_{avg}(t)$, $\boldsymbol{B}_{avg}(t)$, and $\boldsymbol{v}_{avg}(t)$ were calculated for each point using a moving average with a 2 hr window for fast wind and an 8 hr window for slow wind. In order to match the best possible conditions for Alfvénic turbulence, the mean plasma properties were restricted so that the mean bulk speed remains in the range $500 < v_{avg} < 700$ km s^{-1} for fast wind and $280 < v_{avg} < 480$ km s^{-1} for slow wind, $|\delta\boldsymbol{B}|/B_{avg} \leqslant 0.2$ with mean magnetic field magnitude $B_{avg} < 12$ nT and $B_{avg} < 8$ nT for fast and slow wind, respectively, and density fluctuations that are much smaller than the local average density, $\delta\rho/\rho \leqslant 0.15$ to ensure incompressibility. Assuming the turbulence is strong (Goldreich & Sridhar 1995), we estimate the turbulence anisotropy $k_\parallel/k_\perp \sim |\delta\boldsymbol{B}|/B_{avg} \sim 0.2$, and restrict the sampling to be nearly perpendicular to the background field, i.e., $\sin\theta_{VB} \gg 0.2$, where θ_{VB} is the angle between $\boldsymbol{v}_{avg}$ and $\boldsymbol{B}_{avg}$. Based on this condition we restrict the sampling angle to be in the range $50° \leqslant \theta_{VB} \leqslant 130°$.

We invoke the Taylor frozen-in-flow hypothesis (Taylor 1938) to interpret temporal signals as spatial variations, where spatial increments at scale l correspond to temporal increments at timescale $\tau = l/v_{sw}$, where v_{sw} is the mean solar wind speed. Based on this assumption, Equation (1) can be used to calculate increments whenever the conditions described above (to ensure the increment belongs to an Alfvénic interval) are satisfied at the three times, $t - \tau/2$, t, and $t + \tau/2$. Using data from 1995 to 2017, around 1.5×10^6 realizations for fast wind and 1×10^6 realizations for slow wind were obtained.

In order to establish comparisons with observations, we also use pseudospectral simulations of steadily driven, strong balanced reduced MHD turbulence (RMHD) on a rectangular grid with 2048^3 mesh points, which are described in detail in Perez et al. (2012). The simulations describe turbulent Alfvénic fluctuations like those we focus on in observations, with the exception that simulations have zero cross helicity (balanced turbulence or $z^+ \sim z^-$). A total of 30 snapshots of the turbulent fields $\boldsymbol{z}_\alpha(\boldsymbol{x}) = z^\pm(\boldsymbol{x}, t_\alpha)$ with $\alpha = 1, 2, \ldots, 30$ in the steady state are used from the simulations. Spatial field increments perpendicular to the background of the magnetic field are sampled at a random set of N points $\boldsymbol{x}_i$, with $i = 1, 2, \ldots, N$, generating around 2×10^9 realizations, approximately 1000 times more samples than we obtain from observations.

Once increments are calculated for these three systems, empirical PDF of Elsasser increments are constructed from estimated histograms of the statistical samples for each timescale τ in observations and lengthscale l in simulations.
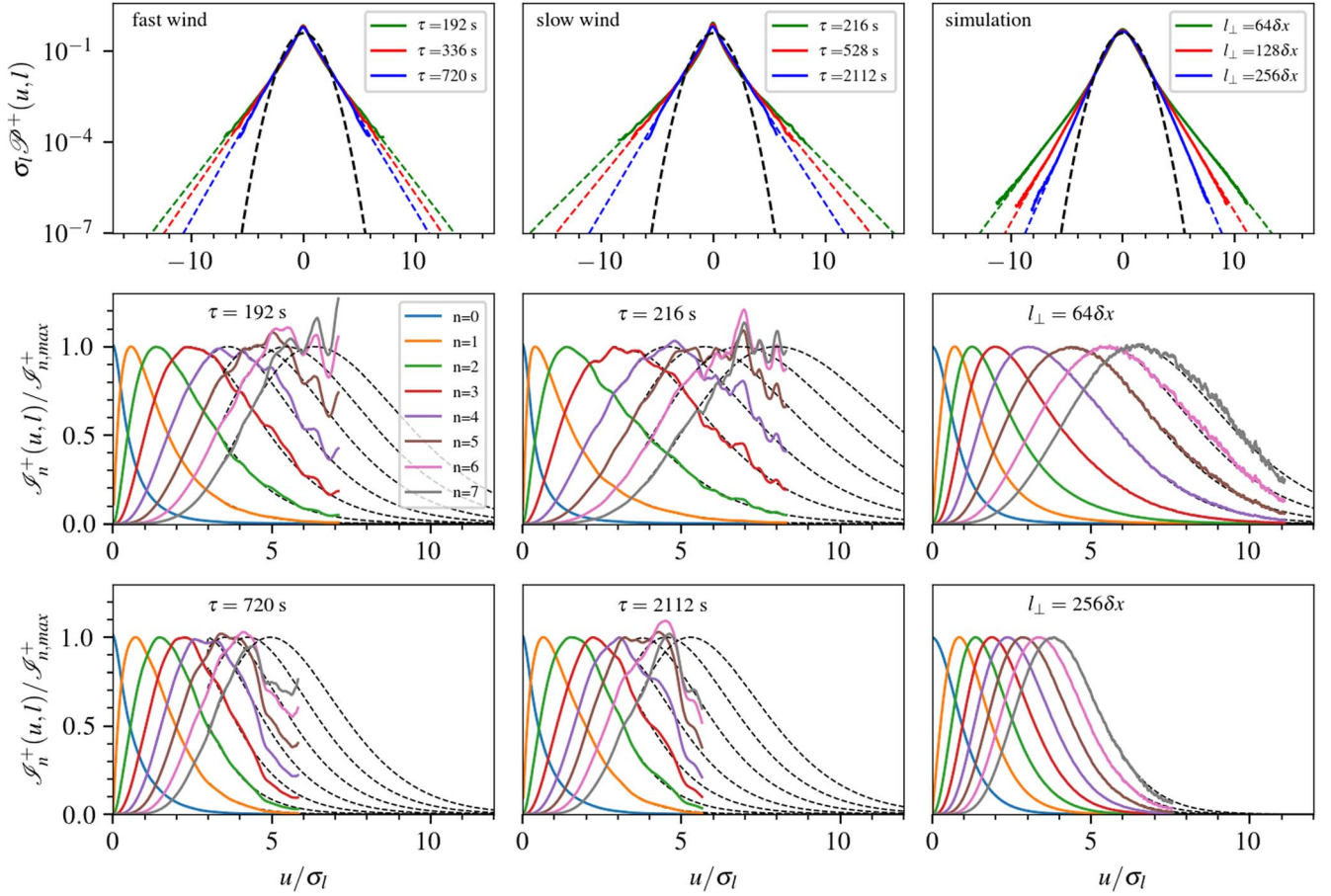
Figure 1. Top panels: continuous lines represent the estimated PDFs $\mathscr{P}^+(u, l)$ vs. u/σ_l for fast wind (left), slow wind (middle), and simulation (right), where $u = \delta z_L^+$. Note that for spacecraft data the space lag is $l = V_{SW}\tau$ via Taylor's Hypothesis, and σ_l represents the standard deviation at scale l. Middle and bottom panels: distribution of nth moment $\mathscr{I}_n^+(u, l)$ normalized to its maximum value ($\mathscr{I}_{n,\max}^+$) for fast wind (left), slow wind (middle), and simulation (right) for two different lags near the end (middle panel) and beginning (bottom panel) of the inertial range. Dashed lines represent the approximation of the PDF extending the tails assuming an exponential behavior.

4. Results and Discussions

Solid lines in Figure 1 show the estimated PDF for the three systems, normalized using the scale-dependent standard deviation σ_l, for three representative scales within the inertial range: near the outer scale (where energy is injected) in green, near the middle of the inertial range in red, and near the dissipation range in blue, while black curves represent a normalized Gaussian for reference. Dashed lines represent an exponential extension of these PDFs. The presence of intermittency becomes evident as the PDF tails become heavier at smaller scales, signifying a departure from self-similarity.

One of the main challenges in the empirical estimation of PDF is that any measurement necessarily involves a finite number of samples, leading to noisy tails, which in turn becomes a source of error in the estimation of statistical averages. In order to reduce the noise, we applied a Savitzky & Golay (1964) filter based on third-order polynomials to each PDF. From our data samples, the resulting PDF cover an increment range of up to 7 standard deviations for fast wind, 10 for slow wind, and 15 for simulations, making them to the best of our knowledge the largest well-defined tails to date (Bruno et al. 1999; Sorriso-Valvo et al. 1999; Sundkvist et al. 2007; Salem et al. 2009; Greco et al. 2010; Alexandrova et al. 2013).

Most empirical results obtained in simulations (Chandran et al. 2015; Mallet et al. 2016) and observations (Bruno 2019)

thus far are only valid for structure functions of low order, i.e., for small values of $n \lesssim 4$ or 5. At a given order n and scale l, $S_n^{\pm}(l)$ represents the area under the curve generated by $\mathscr{I}_n^{\pm}(u, l) = u^n \mathscr{P}^{\pm}(u, l)$, which for convenience we call the distribution of the nth order moment. Empirical estimations of $\mathscr{I}_n^{\pm}(u, l)$ for solar wind observations show that the distribution does not drop to zero fast enough, within the range of measured values, at high order (colored curves in the middle and lower panels of Figure 1), resulting in an underestimation of the corresponding moment, and providing just the first three or four moments with reasonable accuracy. If one assumes that the observed exponential behavior of the tails in the inertial range persists for large increment values (or rare events not captured by the original data), we can use a least-fit square (from 3σ, 3.5σ, and 4.5σ for fast wind, slow wind, and simulations, respectively) to analytically extrapolate the tails as $\propto e^{-\alpha_l |l|}$, where α_l is a positive scale-dependent free parameter describing the tails' exponential decrement.[3]

Interestingly, the exponential decrements $\alpha_l^{\pm}$, shown in Figure 2, exhibit a power-law behavior in the inertial range (indicated by the vertical dashed lines) both in observations and simulations. For fast and slow wind, the scaling exponent for α_l^+ are remarkably similar $\alpha_l^+ \propto l^{-0.25}$ for z^+ increments, while

---

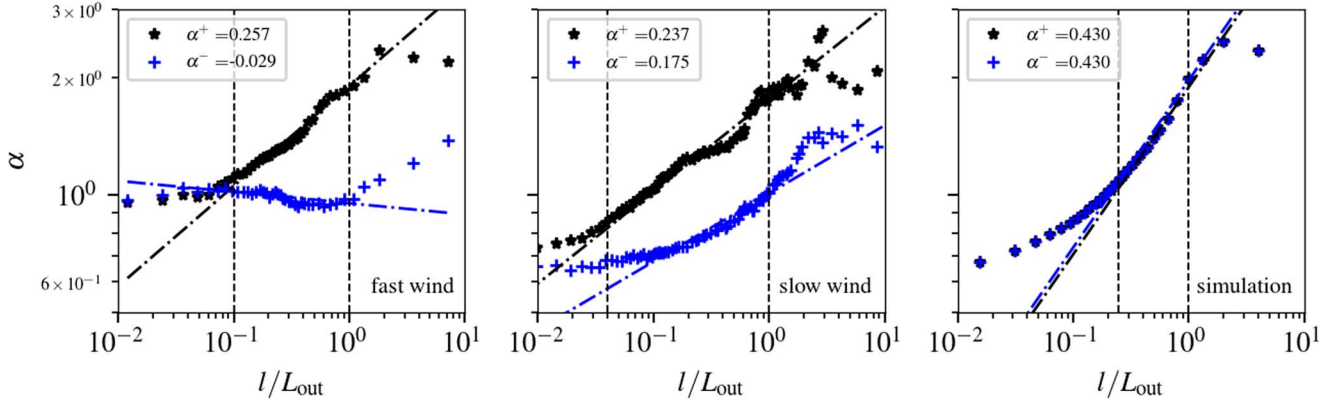[3] In this work we assume the skewness of the PDF is small enough to assume that the tails are nearly symmetric.

Figure 2. Exponential decrements of extended tails α_l for δz_l^+ (black) and δz_l^- (blue) in the fast solar wind (left), slow solar wind (center), and simulation (right). Here l/L_{out} represents the increment scale normalized with respect to the outer scale L_{out} which corresponds to 700 s for fast wind, 2000 s for slow wind, and $256\delta x$ for simulations. Vertical lines represent the limits of the inertial range.

the scaling for z^- increments differs between fast and slow wind. In the former case, it is found that α_l^- is nearly scale-independent, suggesting that z^- increments are less intermittent. For slow wind, the α_l^- power law is slightly flatter than that of α_l^+, suggesting that both z^+ and z^- exhibit intermittent behavior. The power laws that we obtained for the exponential decrement $\alpha_l^{\pm}$ in solar wind measurements are remarkably close to those previously reported in hydrodynamic turbulence from wind tunnel experiments, $\alpha_l \propto l^{-0.17}$, by Praskovsky & Oncley (1994).

In order to obtain better estimates of $S_n^{\pm}(l)$ at high order, under the assumption that the exponential tails extend beyond the measurable range, we use PDF with extrapolated tails, shown by the dashed lines in Figure 1, to numerically evaluate the integral in Equation (4). Figure 3 shows $S_n^+(\tau)$ for $n = 3$ and $n = 10$ for slow wind calculated using the PDF directly constructed from observations (black stars) and PDF with extrapolated exponential tails (blue stars). The overlap between black and blue stars in the top panel shows, as expected, that using either PDF to estimate S_3 leads to the same result. The bottom panel shows that S_{10} is underestimated at each scale when the empirical PDF is used vs the extrapolated one. Remarkably, its inertial-range scaling remains nearly identical for both PDFs, suggesting that at each scale S_{10} estimated from the empirical PDF represents the same fraction of its estimate with the extrapolated one. A similar result was observed in neutral fluid experiments by Anselmet et al. (1984) up to order $n = 18$.

We identify the inertial range as the region where its power-law fit (black line) intersects the corresponding fits in the dissipation (green line) and outer scale (red line) ranges. Using this method we identify the inertial range from 200 to 2000 s for slow wind, from 200 to 700 s for fast wind, and $64\delta x$ to $256\delta x$ where δx represents the grid size in simulations. In order to determine the scaling exponents more accurately we use the so-called Extended Self Similarity (ESS; Benzi et al. 1993). For reasons that are still not well understood, plotting $S_n^{\pm}$ as a function of $S_3^{\pm}$ instead of l leads to extended power-law scaling, even outside the inertial range. The reason why Benzi et al. (1993) selected S_3 is because this is proportional to the scale size in hydrodynamics. Although for MHD, turbulence $S_3^{\pm}$ is not necessarily proportional to l, it has also been found that using ESS leads to extended power-law regions. The only disadvantage is that scaling exponents $\gamma_n^{\pm}$ measured from ESS
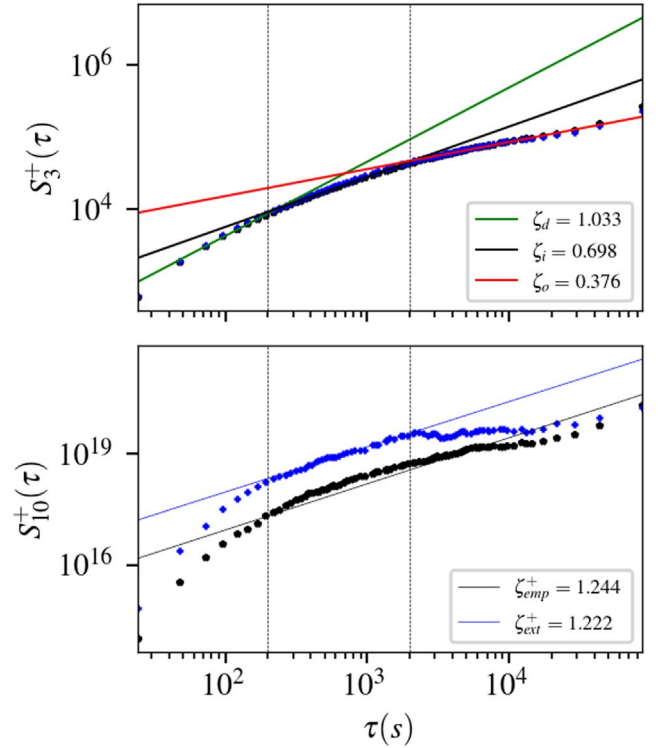

Figure 3. Third (top) and tenth (bottom) order structure functions for δz^+ of slow wind calculated using the empirical PDF (black marks) and the extrapolated PDF using exponential tails (blue marks) vs. time lags. Green and red lines show power-law fits for the dissipative and injection regions, respectively, while the black vertical lines indicate the lower and upper limits of the inertial range.

are related to $\zeta_n^{\pm}$ as $\gamma_n^{\pm} = \zeta_n^{\pm}/\zeta_3^{\pm}$, which still requires an accurate estimation of $\zeta_3^{\pm}$.

Figure 4 shows the scaling exponents of structure functions up to order $n = 12$ for δz^+ and δz^- using ESS for the three systems, namely, the fast and slow wind as well as simulations. The scaling exponents ζ_n^+ are represented by black symbols and ζ_n^- by red symbols, while those exponents resulting from the empirical PDF are represented by star symbols and those resulting from the empirical PDF are represented by diamonds. With the exception of ζ_n^- in fast wind (left panel) all scaling exponents are nonlinear in n, which suggests multifractal behavior.
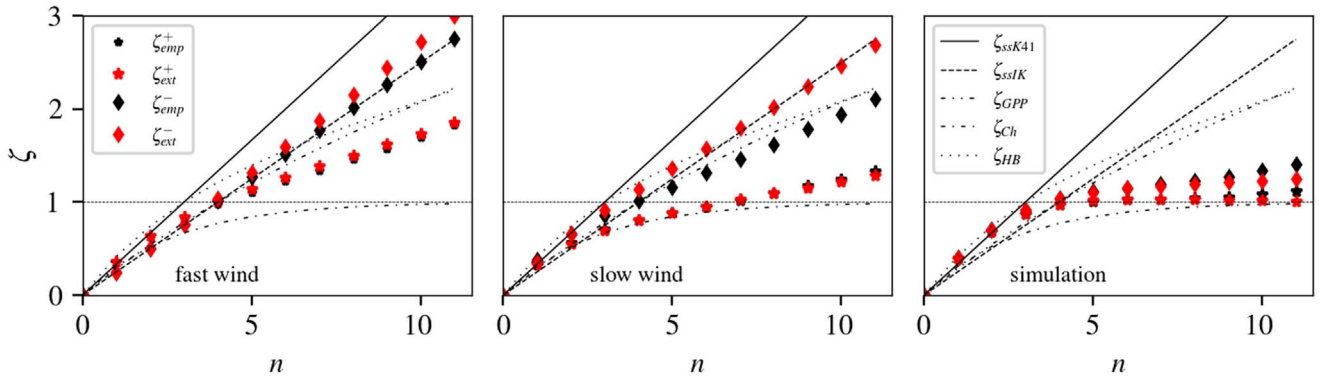
Figure 4. Scaling exponents for δz_L^+ and δz_L^- increments for fast wind (left), slow wind (middle), and simulation (right) directly calculated with the experimental data (ζ_e) and using the PDF modeled with exponential tails (ζ_m). ESS is applied in all cases.

One of the most successful multifractal models in hydrodynamic turbulence was presented by She & Leveque (1994), based on log–Poisson distributions, which was later extended by Horbury & Balogh (1997) to MHD turbulence for K41 scaling ($h = 1/3$)

$$\zeta_n^{\mathrm{HB}} = \frac{n}{9} + 1 - \left(\frac{1}{3}\right)^{n/3}, \qquad (5)$$

and by Grauer et al. (1994) and Politano & Pouquet (1995) for the IK scaling ($h = 1/4$)

$$\zeta_n^{\mathrm{GPP}} = \frac{n}{8} + 1 - \left(\frac{1}{2}\right)^{n/4}. \qquad (6)$$

These models are of particular interest because they contain no freely adjustable parameters. More recently, Chandran et al. (2015) proposed a new model based on Alfvén wave collisions, assuming that each balanced collision reduces a fluctuation's amplitude by a constant factor $\beta \simeq 0.691$, leading to a simple relation for the scaling exponents,

$$\zeta_n^{\mathrm{CH}} = 1 - \beta^n. \qquad (7)$$

A similar result was obtained by Mallet & Schekochihin's (2017) phenomenological model with $\beta = 0.7$.

Figure 4 shows comparisons between empirical results and the following theoretical predictions: the self-similar models with $h^\pm = 1/3$ (ssK41) and $h^\pm = 1/4$ (ssIK) in Equation (3), Horbury and Balogh (HB), Grauer et al., Politano and Pouquet (GPP) and Chandran et al. (CH) models in Equations (5), (6) and (7) respectively. For ζ_n^+, we observe that up to $n = 12$ the values estimated from the empirical PDF (or the standard method) are very close to those obtained with extrapolated PDF. The multifractal behavior of ζ_n^+ is evident in the strong departure from self-similarity in all three cases. In contrast, ζ_n^- shows little departure from self-similarity and is very close to the ssIK model calculated using PDFs with an extrapolated tail. As opposed to ζ_n^+, our results also show that for high orders the scaling exponents ζ_n^- are in fact different when the PDF tails are extrapolated. The exponent of S_4^+ for fast wind is very close to 1, suggesting that $\langle \delta z^+ \rangle \propto l$, consistent IK scaling. For slow wind, the first six scaling exponents are remarkably close to the CH model. In contrast to observations, ζ^+ and ζ^- are very similar in simulations because they correspond to a steady state of balanced turbulence, in which Elsasser variables have comparable amplitudes.

5. Conclusions

Accurate measurements of structure functions provide critical information about the development of intermittency and help to understand the energy transfer in the inertial range. In this Letter we proposed a methodology to obtain Elsasser increments that allows us to collect the largest possible statistics of Alfvénic solar wind for fast and slow wind. The statistics were large enough that we were able to construct PDF of increments at each scale spanning up to 7 and 10 standard deviations for fast and slow wind, respectively, with less noisy and statistically better-defined tails than previous works (Bruno et al. 1999; Sorriso-Valvo et al. 1999; Sundkvist et al. 2007; Salem et al. 2009; Greco et al. 2010; Alexandrova et al. 2013; Osman et al. 2014).

Proper estimation of high-order structure functions requires accurate estimations of the PDF tails. However, this is normally not possible with a finite statistical sample, as they rely on rare events. Because of our substantially large statistical sample obtained through conditioning of 23 yr of observations ($\sim 10^6$ samples) and an even larger sample in simulations ($\sim 10^9$), we were able to identify exponential tail behavior over several standard deviations in the inertial range, with an exponential decrement that satisfies well-defined power-law behavior of the form $\alpha_l \propto l^{-\mu}$, with μ between 0.17 and 0.25 for observations and 0.43 for simulations. This observed scaling of the exponential decrement, not previously reported in the solar wind literature, is very similar to those observed in fluid experiments, suggesting that this is potentially an intrinsic (or universal) property of the PDF of Elsasser increments. If this exponential behavior persists well beyond the measurable range, it could help us obtain a deeper understanding of intermittency in the solar wind, such as the scaling of high-order structure functions beyond the limit imposed by empirical data with a finite sample.

Under the assumption that in the inertial range the behavior of the tails remains exponential beyond the maximum measurable increment, as observed in simulations, we extrapolated the PDFs as long as needed to improve calculations of structure functions and the corresponding scaling exponents. The scaling exponent of S_3 in the inertial range is observed to be smaller than unity for both Elsasser increments in the three experiments, suggesting a deviation from K41 theory and similar models. The scaling exponents ζ^+ confirm the multifractal nature of δz^+ increments. Although none of the models presented in Section 4 fully describes the behavior of exponents for δz^+ in all three systems, we found that for fast

wind observations S_4 has a value very close to 1, consistent with IK scaling, while for slow wind, the first moments are very close to those predicted by CH model, and substantially deviates from observations for $n > 6$. For δz^-, both fast and slow wind reveal self-similar behavior with $h = 1/4$ using PDFs with extrapolated tails, which can potentially shed some light on the possible sources of these fluctuations.

ORCID iDs

Juan C. Palacios ⓘ https://orcid.org/0000-0002-3249-3335
Sofiane Bourouaine ⓘ https://orcid.org/0000-0002-2358-6628
Jean C. Perez ⓘ https://orcid.org/0000-0002-8841-6443

References

Alexandrova, O., Chen, C. H. K., Sorriso-Valvo, L., Horbury, T. S., & Bale, S. D. 2013, SSRv, 178, 101
Anselmet, F., Gagne, Y., Hopfinger, E. J., & Antonia, R. A. 1984, JFM, 140, 63
Barndorff-Nielsen, O. E., Blæsild, P., & Schmiegel, J. 2004, EPJB, 41, 345
Belcher, J. W., Davis, L., Jr, & Smith, E. J. 1969, JGR, 74, 2302
Benzi, R., Ciliberto, S., Tripiccione, R., et al. 1993, PhRvE, 48, R29
Beresnyak, A., & Lazarian, A. 2008, ApJ, 682, 1070
Biskamp, D., & Müller, W.-C. 2000, PhPl, 7, 4889
Boldyrev, S. 2005, ApJL, 626, L37
Bruno, R. 2019, E&SS, 6, 656
Bruno, R., Bavassano, B., Pietropaolo, E., Carbone, V., & Veltri, P. 1999, GeoRL, 26, 3185
Bruno, R., & Carbone, V. 2013, LRSP, 10, 2
Burlaga, L. F. 1991, JGRA, 96, 5847
Chandran, B. D. G. 2008, ApJ, 685, 646
Chandran, B. D. G., Schekochihin, A. A., & Mallet, A. 2015, ApJ, 807, 39
Coleman, P. J., Jr. 1968, ApJ, 153, 371
Elsasser, Walter M. 1950, PhRv, 79, 183
Goldreich, P., & Sridhar, S. 1995, ApJ, 438, 763
Gotoh, T., Fukayama, D., & Nakano, T. 2002, PhFl, 14, 1065
Grauer, R., Krug, J., & Marliani, C. 1994, PhLA, 195, 335
Greco, A., Servidio, S., Matthaeus, W., & Dmitruk, P. 2010, P&SS, 58, 1895
Horbury, T. S., & Balogh, A. 1997, NPGeo, 4, 185
Iroshnikov, P. S. 1963, AZh, 40, 742
Iroshnikov, P. S. 1964, SvA, 7, 566
Kolmogorov, A. N. 1941a, RSPSA, 434, 15
Kolmogorov, A. N. 1941b, RSPSA, 434, 9
Kraichnan, R. H. 1965, PhFl, 8, 1385
Lithwick, Y., Goldreich, P., & Sridhar, S. 2007, ApJ, 655, 269
Mallet, A., & Schekochihin, A. A. 2017, MNRAS, 466, 3918
Mallet, A., Schekochihin, A. A., Chandran, B. D. G., et al. 2016, MNRAS, 459, 2130
Osman, K. T., Kiyani, K. H., Chapman, S. C., & Hnat, B. 2014, ApJ, 783, L27
Perez, J. C., & Boldyrev, S. 2009, PhRvL, 102, 025003
Perez, J. C., Mason, J., Boldyrev, S., & Cattaneo, F. 2012, PhRvX, 2, 041005
Politano, H., & Pouquet, A. 1995, PhRvE, 52, 636
Praskovsky, A., & Oncley, S. 1994, PhRvL, 73, 3399
Salem, C., Mangeney, A., Bale, S. D., & Veltri, P. 2009, ApJ, 702, 537
Savitzky, A., & Golay, M. J. E. 1964, AnaCh, 36, 1627
She, Z.-S., & Leveque, E. 1994, PhRvL, 72, 336
Sorriso-Valvo, L., Carbone, V., Veltri, P., Consolini, G., & Bruno, R. 1999, GeoRL, 26, 1801
Sundkvist, D., Retinò, A., Vaivads, A., & Bale, S. D. 2007, PhRvL, 99, 025004
Taylor, G. I. 1938, RSPSA, 164, 476
Zhdankin, V., Boldyrev, S., & Uzdensky, D. A. 2016, PhPl, 23, 055705